Journal of Magnetic Resonance 209 (2011) 233–243

Contents lists available at ScienceDirect

Journal of Magnetic Resonance

journal homepage: www.elsevier.com/locate/jmr

Enhancing time-suspension sequences for the measurement of weak perturbations

Matthew R. Tarasek, David J. Goldfarb, James G. Kempf *

Department of Chemistry & Chemical Biology, Center for Biotechnology and Interdisciplinary Studies, Rensselaer Polytechnic Institute, Troy, NY 12180, United States

ARTICLE INFO

Article history:
Received 23 November 2010
Revised 8 January 2011
Available online 21 January 2011

Keywords:
Time suspension
Multiple-Pulse Line Narrowing
Second averaging
Phase stepping
Power compensation
POWER NMR

ABSTRACT

We detail key features for implementation of time-suspension multiple-pulse line-narrowing sequences. This sequence class is designed to null the average Hamiltonian ($\overline{\mathcal{H}}^{(0)}$) over the period of the multiple-pulse cycle, typically to provide for high-resolution isolation of evolution from a switched interaction, such as field gradients for imaging or small sample perturbations. Sequence designs to further ensure null contributions from correction terms ($\overline{\mathcal{H}}^{(1)}$ and $\overline{\mathcal{H}}^{(2)}$) of the Magnus expansion are also well known, as are a variety of approaches to second averaging, the process by which diagonal content is incorporated in $\overline{\mathcal{H}}^{(0)}$ to truncate unwanted terms. In spite of such designs, we observed spin evolution not explicable by $\overline{\mathcal{H}}^{(0)}$ using 16-, 24- and 48-pulse time-suspension sequences. We found three approaches to effectively remove artifacts that included splitting of the lineshape into unexpected multiplets as well as chirped evolution. The noted approaches are simultaneously compatible for combination of their benefits. The first ensures constant power deposition from RF excitation as the evolution period is incremented. This removes chirping and allows more effective 2nd averaging. Two schemes for the latter are evaluated: the noted introduction of a diagonal term in $\overline{\mathcal{H}}^{(0)}$, and phase-stepping the line-narrowing sequence on successive instances during the evolution period. Either of these was sufficient to remove artifactual splittings and to further enhance resolution, while in combination enhancements were maintained. Finally, numerical simulations provide evidence that our experimental line-narrowing results with ^{75}As in crystalline GaAs approach performance limits of idealized sequences (e.g., with ideal square pulses, etc.). The three noted experimental techniques should likewise benefit ultimate implementation with switched interactions and corresponding new error contributions, which place further demand on sequence performance.

1. Introduction

Multiple-Pulse Line Narrowing (MPLN) is a widely used technique in NMR spectroscopy and imaging. It mitigates the impact of undesirable interactions on nuclear spin evolution. Pulses applied in cyclic fashion selectively average certain spin Hamiltonians to near zero over the period of the sequence [1]. Typically, at least one spin Hamiltonian is averaged to a finite value to produce measurable spin evolution free from inhomogeneities of the nulled interactions. The WaHuHa 4-pulse sequence (WHH-4) is perhaps most famous in this regard [2], along with MREV-8 [3,4], BR-24 [5] and Cory's 48-pulse sequence (DC-48) [6]. Each retains scaled chemical-shift evolution, while removing the largely dipolar contributions to linewidth. In contrast, time-suspension sequences null all spin Hamiltonians, including chemical-shift, dipolar and quadrupolar interactions. Their purpose is to remove the background for spectra obtained with an additional switched interaction for imaging. Most commonly, field gradients applied in select windows of a time-suspension cycle allow imaging of the distribution of spins via spatially dependent evolution from the MPLN sequence (plus gradients) during an indirect dimension (t_1) [7–12]. More recently, the concept has been extended to include imaging switched perturbations to the sample. For example, hyperfine or quadrupolar Stark effects (QSEs) introduced by MPLN-synchronized optical excitation of localized electrons [13,14], or QSEs in response to similarly synchronized external electric fields [15–17].

For imaging with time-suspension and related applications of shift-retaining sequences, suppression of ^{1}H–^{1}H dipolar couplings has been paramount. Experiments designed for the latter category (WHH-4, etc.) have thus far proven to be robust in minimizing the dipolar background in solid-state contexts ranging from organic polymers to large biomolecules. For imaging, successful time-suspension sequences include the 16-pulse CLSW-16 [7], two 24-pulse cycles from either Lenovsky and Weitekamp (LW-24) [18,19] or Cory et al. [9], and the 48-pulse cycle (CMG-48) also from Cory, et al. Sequences from this set have given reasonably similar proton linewidths from a variety of solid-state small-molecule or polymeric samples [9]. Although performance did correlate with sequence complexity (i.e., number of pulses and pattern of

* Corresponding author. Address: RPI, Department of Chemistry, 110 8th Street, 209a Cogswell Lab, Troy, NY 12180, United States. Fax: +1 518 276 4887.
E-mail address: kempfj2@rpi.edu (J.G. Kempf).

1090-7807/$ - see front matter © 2011 Elsevier Inc. All rights reserved.
doi:10.1016/j.jmr.2011.01.016

their phases). Such complexity was designed to zero ever higher-order terms in the Magnus expansion of average Hamiltonian theory (AHT), most notably $\overline{\mathcal{H}}_D^{(2)}$, the 2nd-order contribution from homonuclear dipolar interactions including the effects of finite pulse times. Further enhancements from 2nd-averaging are also well known [1,8,20,21]. Generally, that approach is to modify the MPLN sequence to yield a non-zero average Hamiltonian ($\overline{\mathcal{H}}^{(0)} \neq 0$) that is orthogonal to expected error terms. In that way, $\overline{\mathcal{H}}^{(0)}$ may truncate unwanted terms, much like the common secular approximation is truncation by the Zeeman interaction. By combining 2nd averaging with sophisticated 'first' averaging from unmodified time-suspension sequences, dramatic resolution gains of 10^3–10^4 orders of magnitude in ^{1}H linewidth have been the norm [7–9].

In spite of design quality and utility of time-suspension sequences for gradient-based imaging, additional improvements are needed. This is especially apparent for the newer class of experiments to image small perturbations to the sample. POWER (Perturbations Observed With Enhanced Resolution) NMR presents unique concerns for line-narrowing performance. First, while compatible with ^{1}H NMR, the POWER approach is not solely focused on abundant, high-γ spins (protons) for imaging. Thus, MPLN with spins >½ is of interest. Secondly, the switched interaction of POWER NMR may not conveniently commute with the toggling-frame I_z, in contrast to gradient-based imaging. For example, one scheme offers conversion of a switched $I_{\pm}^2$ quadrupolar interaction to I_z^2 [15,16]. This complicates AHT treatment of the switched interaction, of intrinsic Hamiltonians, and of cross terms between the two. Essentially, selective introduction of a perturbation (p) may provide the desired $\overline{\mathcal{H}}_p^{(0)}$, but may also yield new error terms, $\overline{\mathcal{H}}_{pX}^{(0)}$ and $\overline{\mathcal{H}}_X^{(n)}$ ($n > 0$) for 'X' an intrinsic interaction. These can dethrone $\overline{\mathcal{H}}_p^{(0)}$ as the dominant source of evolution or, at the least, hasten decay of the desired signal.

In this paper, we explore a broader array of techniques for improved time-suspension averaging. Importantly, these remove the effects of unwanted contributions, $\overline{\mathcal{H}}^{(n)}$, in redundant fashion. That is, via simultaneous application of distinct approaches for error removal, each of which would have been sufficient on its own. Such 'redundancy' may turn instead to necessity when moving from 'bare-sequence' performance to the measurement of switched interactions. First, we demonstrate a simple technique to ensure the temporal homogeneity of the averaging process. That is, the effect of the sequence must not vary as the evolution period (t_1) during which it is repetitively applied is incremented. This has proven a key practical issue, yielding severe lineshape distortions (chirped signals). As simple remedy, we employed a constant-power format, wherein the sequence was also applied during a pre-recycle-delay period that decreased in duration as t_1 and its component MPLN cycles increased. This was essential, as observed chirping was nearly immune to 2nd averaging. In fact, without power compensation, the utility of the latter was lost due to increasing distortion with the magnitude of the 2nd-averaging Hamiltonian.

Next, we detail enhancements from two 2nd-averaging techniques whose simultaneous effect removes unwanted spectral artifacts (splittings) and reduces linewidth. The first of these is the noted introduction of $\overline{\mathcal{H}}^{(0)} \neq 0$, and the second is to 'phase step' the MPLN sequence by 90° on each successive application during t_1. The stepping does not alter $\overline{\mathcal{H}}^{(0)}$ of the bare sequence (hence, leaving the zero-order description of evolution intact). However, it does reorient error contributions such that their net effects vanish over the period of the phase step. This method is fully compatible with imaging or POWER NMR applications. There, care must be taken to incorporate the switched interaction (p) such that $\overline{\mathcal{H}}_p^{(0)}$ does not vary with phase steps. This requires, at most, stepping its polarity or phase in concert with the MPLN sequence. For example, phase stepping does not affect the zeroth-order description of a switched *static* field gradient or *static* E field.[1] However, when instead using *RF* gradients or E fields, the phase of the switched interaction must be stepped to maintain constant $\overline{\mathcal{H}}_p^{(0)}$. Finally, the simple technique of phase stepping may have precedent in the formal literature, but we have not found a presentation matching our current implementation. However, we note inspiration from the thesis by Werner with Weitekamp, which briefly suggested the approach in simulations of imaging sequences with RF gradients. (See p. 83 of Ref. [19].) In addition, distinct phase modulation schemes are widely used in other refocusing contexts, such as supercycles formed from inverted and reordered sequence elements [22,23].

Here, we found that, individually, either traditional or phase-stepped approaches to 2nd averaging fully removed unwanted splittings and/or doubled resolution enhancement. When using the two methods in concert, results indicate full compatibility but no further enhancements. Ultimately, we anticipate that combined application of these two techniques, all in constant-power format, will enhance performance in the face of new challenges from POWER NMR. Finally, we employed numerical simulations of MPLN performance with two aims: (1) to explore the extent to which our experiments achieve the relative ideality of simulation, and (2) to prove the numerical approach with 'bare' time-suspension sequences as a benchmark for subsequent simulations with switched perturbations. We begin Results and Discussion by detailing the need for and benefits of power compensation. From there, we describe results with our combination of 2nd-averaging techniques using CLSW-16, LW-24 and CMG-48. Finally, we present the simulation framework and evaluate predicted vs. observed performance.

2. Materials and methods

2.1. Sample and apparatus

A single-crystal, high-resistivity, undoped GaAs sample from El-Cat, Inc. (Waldwick, NJ) was used. All relevant sample characteristics were described earlier (sample 'A' of Ref. [17]). Briefly, the sample was 350 μm thick with crystal [001] axis normal to the sample surface. We used an approximately 2 mm × 4 mm section cut from the purchased wafers.

All experiments were performed on a Bruker Avance III wide-bore solid-state NMR spectrometer at B_0 = 14.1 T. The ^{75}As signal from our samples was at $\omega_0/(2\pi) \sim 102.787$ MHz, or about −77 ppm relative to AsF_6^- (though direct referencing was not applied). The sample was centered in the NMR coil in a sandwich of Kapton tape. Its temperature was maintained at 296 K by gentle flow (~8 L/min) of nitrogen taken from ballast tanks of *l*-N_2 storage. Other details of our apparatus were described earlier [16,17], although the home-built probe was updated here (a) for B_1 excitation and detection of ^{75}As and (b) by removal of previously relevant apparatus for excitation by a radiofrequency E field. The main probe update concerns the B_1 coil, here a solenoid wound from 20 gauge copper wire with 11.5 turns and 7 mm inner diameter. As a marker of corresponding B_1 homogeneity within our sample, typical observation yielded $a_{90}/a_{810} > 0.97$, where a_{90} was signal amplitude from a single 90° pulse ($t_p = t_{90}$) and a_{810} was that from a pulse $t_p = 9t_{90}$.

[1] To illustrate, consider that phase steps are a 'rotation' of the pulse sequence about I_z such that individual pulse propagators (U_{rf}) from the unstepped sequence become $e^{-i\phi_{MPLN}I_z}U_{rf}e^{+i\phi_{MPLN}I_z}$. It is then straightforward to show that toggling-frame transformations ($I_{z,T}$) of I_z are independent of ϕ_{MPLN} for any window in which $I_{z,T} = \pm I_z$. Exactly these operators and windows are used for imaging with static gradients, or for POWER NMR with static E fields, hyperfine shifts or other I_z-based interaction.

2.2. NMR experiments: general features

Real-time (t_2) signal transients were collected at 100 kHz spectral width for 1.55 ms acquisition time using digital quadrature detection. In all experiments, a recycle delay of 1.5 s was used and the $\pi/2$ time for ^{75}As was 4.0 μs at 150.3 W power. Fourier transformation of individual transients yielded a Gaussian spectrum with FWHM of 2.24 ± 0.02 kHz. The longitudinal spin-relaxation time (for single exponential fits) for our conditions was $T_1(^{75}\mathrm{As}) = 234 \pm 5$ ms. Use of single-exponentials was justified previously [17], in spite of distinct contributions expected from quadrupolar fluctuations at ω_0 and $2\omega_0$.

2.3. Multiple-Pulse Line Narrowing (MPLN)

The general MPLN scheme is given in Fig. 1a. An optional power-compensation period precedes the recycle delay (d_1), and is executed $(n_{\max} - n) \times n_{incr}$ times, where $n \le n_{\max}$ is the index of the current t_1 point and n_{incr} is the number of MPLN cycles per increment of $t_1 = n \times n_{incr} \times t_{cyc}$. When neglecting power compensation, pulses in the corresponding period of Fig. 1a were replaced by delays. When applying phase stepping to the MPLN sequence in t_1, each successive application of the sequence was incremented by 90°, i.e., $\phi_{\mathrm{MPLN}} = 0°$, 90°, 180°, 270°, where the 0° starting case

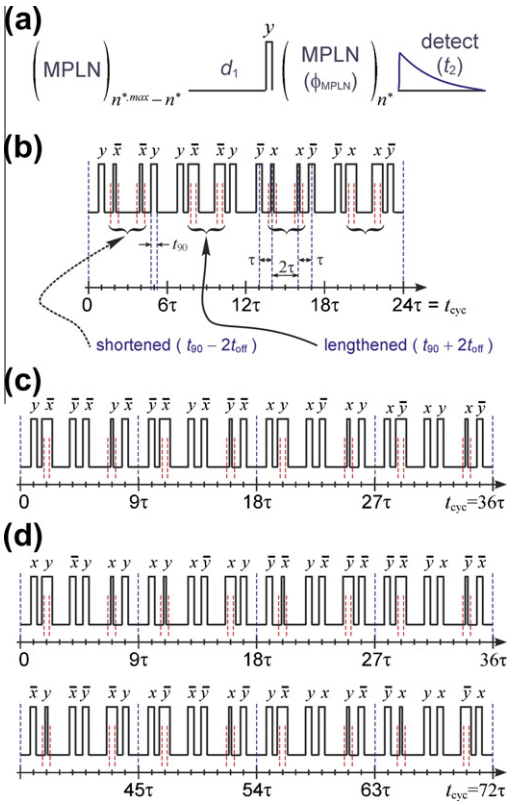

Fig. 1. MPLN with power compensation, homogeneous offsets and phase stepping. (a) General experiment timeline, with power-compensation period preceding recycle delay (d_1). The MPLN sequence may be implemented with phase stepping, in which case ϕ_{MPLN} is added to each member pulse on successive instances. Phases during power compensation are inconsequential. (b) CLSW-16 sequence including symmetric modifications ($\pm 2t_{off}$) to timings of selected pulses, which provides uniform frequency offset and 2nd averaging. [Short, dashed lines clarify all pulse-width modifications, whereas arrows to short/long text labels highlight only a subset of such.] Note, solid-echo pulse spacings are (τ–$t_p/2$). (c) Similar depiction of LW-24. (d) CMG-48, each with its own unique pattern of pulse-width modifications for offset and 2nd averaging. For convenience of viewing, the LW-24 and CMG-48 sequences are demarked with dashed lines in six-pulse groups. The CMG-48 timeline (0–72τ) is broken across two lines.

Table 1
Toggling-frame representation of CLSW-16. The average Hamiltonian of any spin interaction is determined by the progression of noted basis operators. Starred (*) values where $I_x \to I_z$ transformation is utilized with pulse modifications t_{off} to obtain $\overline{\mathcal{H}}^{(0)}_{off} \propto I_z$. [For details, see Supporting Information.]

Window	Basis ops			Quad-echo group		Window duration
	I_x	I_y	I_z			
0	I_x	I_y	I_z	A		τ
1	$-I_z^*$	I_y	I_x	B		τ
2	$-I_z^*$	$-I_x$	I_y	C	C	2τ
3	$-I_z^*$	$-I_y$	$-I_x$		−B	τ
4	I_x	$-I_y$	$-I_z$	−A	−A	2τ
5	I_z^*	$-I_y$	I_x	B		τ
6	I_z^*	$-I_x$	$-I_y$	−C	−C	2τ
7	I_z^*	I_y	$-I_x$		−B	τ
8	I_x	I_y	I_z	A	A	2τ
9	I_z^*	I_y	$-I_x$	−B		τ
10	I_z^*	$-I_x$	$-I_y$	−C	−C	2τ
11	I_z^*	$-I_y$	I_x		B	τ
12	I_x	$-I_y$	$-I_z$	−A	−A	2τ
13	$-I_z^*$	$-I_y$	$-I_x$	−B		τ
14	$-I_z^*$	$-I_x$	I_y	C	C	2τ
15	$-I_z^*$	I_y	I_x		B	τ
16	I_x	I_y	I_z		A	τ

corresponds to pulse phases given in Fig. 1b–d for CLSW-16 [7], LW-24 [18,19] and CMG-48 [9]. The phases for LW-24 were reverse-engineered from reported [19] 'ABC' notation that tracked the toggling-frame state of I_z. Finally, phase-stepping with 'substep' sampling (e.g., $n_{incr} = 1$) yielded equivalent performance (and 4 × spectral width) than in the case most typically employed here ($n_{incr} = 4$). Current limitations of the pulse-sequence handler in incrementing phase pointers usually made the latter choice more convenient, while also providing time savings at cost of (presently unneeded) spectral width.

In exploring line-narrowing performance of each MPLN sequence (a) with and without power compensation, and (b) with and without phase stepping, we further tested each case vs. (c) 2nd averaging provided by modifications (t_{off}) to the durations of selected pulses. This shifts the NMR signal in t_1 from zero frequency, yielding $\nu_{off} \propto t_{off}$. Patterns of pulse-timing offsets for the three noted time-suspension sequences are shown in Fig. 1b–d. These patterns are independent of phase stepping. [See Supporting information (SI).] The arrangement for CLSW-16, with symmetrically placed modifications ($\pm 2 \times t_{off}$) to selected pulse durations, was described previously [16,24], and is based on the original implementation of the sequence for imaging with RF field gradients [7]. The patterns of modified pulse times shown for LW-24 and CMG-48 have not, to our knowledge, been suggested previously, whereas Cory et al. [8,9] generate a distinct 2nd-averaging Hamiltonian using 'phase-toggling'.[2] We derived the schemes of Fig. 1c and d by straightforward extension the design principles applied with CLSW-16. For each noted sequence, the modifications contribute

$$\left|\overline{\mathcal{H}}^{(0)}_{off}\right| = n_{p,mod}(2t_{off}/t_{cyc})\nu_1 I_z \qquad (1)$$

to the average Hamiltonian in t_1, where $n_{p,mod}$ is the number of appropriately modified pulses in an MPLN sequence of duration t_{cyc}, and ν_1 is the Rabi frequency in Hz.[3] Eq. (1) is readily derived from the toggling-frame operator states of the three sequences, provided in Tables 1–3. [See also, Tables S1–S3 of SI, which give modified

[2] Phase toggling, the intentional missetting of select pulse phases within an MPLN sequence, is distinct from phase stepping employed here.

[3] Only the magnitude of $\overline{\mathcal{H}}^{(0)}_{off}$ is important for 2nd averaging and the sign of $\overline{\mathcal{H}}^{(0)}_{off}$ may be flipped by swapping lengthened and shortened pulse modifications. As depicted in Fig. 1, CLSW-16 yields negative $\overline{\mathcal{H}}^{(0)}_{off}$, whereas the other two sequences carry a positive sign.

Table 2
Toggling-frame representation of LW-24, starred values similar to Table 1.

Window	Basis ops			Quad-echo group		Window duration
	I_x	I_y	I_z			
0	I_x	I_y	I_z	A		τ
1	$-I_z^*$	I_y	I_x	B		τ
2	$-I_z^*$	$-I_x$	I_y	C	C	2τ
3	I_y	$-I_x$	I_z		A	τ
4	I_y	$-I_z^*$	$-I_x$	−B	−B	2τ
5	I_x	$-I_z^*$	I_y	C		τ
6	I_x	$-I_y$	$-I_z$	−A	−A	2τ
7	$-I_z^*$	$-I_y$	$-I_x$		−B	τ
8	$-I_z^*$	I_x	$-I_y$	−C	−C	2τ
9	I_y	I_x	$-I_z$	−A		τ
10	I_y	$-I_z^*$	I_x	B	B	2τ
11	I_x	$-I_z^*$	$-I_y$		−C	τ
12	I_x	I_y	I_z	A	A	2τ
13	I_x	$-I_z^*$	$-I_y$	−C		τ
14	I_y	$-I_z^*$	I_x	B	B	2τ
15	I_y	I_x	$-I_z$		−A	τ
16	$-I_z^*$	I_x	$-I_y$	−C	−C	2τ
17	$-I_z^*$	$-I_y$	$-I_x$	−B		τ
18	I_x	$-I_y$	$-I_z$	−A	−A	2τ
19	I_x	$-I_z^*$	I_y		C	τ
20	I_y	$-I_z^*$	$-I_x$	−B	−B	2τ
21	I_y	$-I_x$	I_z	A		τ
22	$-I_z^*$	$-I_x$	I_y	C	C	2τ
23	$-I_z^*$	I_y	I_x		B	τ
24	I_x	I_y	I_z		A	τ

toggling-frame states vs. ϕ_{MPLN} and discuss the invariance of $\left|\overline{\mathcal{H}}_{off}^{(0)}\right|$ vs. ϕ_{MPLN}.] When $\left|\overline{\mathcal{H}}_{off}^{(0)}\right|$ is the sole contribution to $\overline{\mathcal{H}}^{(0)}$, a single peak is expected at frequency

$$|\nu_{off}| = n_{p,mod}(2t_{off}/t_{cyc})\nu_1 \quad (2)$$

For designs of both CLSW-16 and LW-24 in Fig. 1b and c, we have $n_{p,mod} = 8$, whereas CMG-48 in Fig. 1d has $n_{p,mod} = 16$. Thus, on a per-total-pulses basis at identical RF duty factors, CLSW-16 provides 1.5-fold higher offset frequency than either LW-24 or CMG-48.

We tested MPLN performance vs. t_{off} values ranging from 0 to ~1600 ns (typically ~0, 20, 40, 60, 100, 150, 300, 600, 900, 1200, and 1600 ns), where unmodified pulse times were $t_p = 4.0$ μs. Effort was made to avoid choosing t_{off} values that would place true or aliased frequencies at zero or either Nyquist frequency. Likewise, some experiments included TPPI [25] of the $\pi/2$ prep pulse by 90° on each t_1 increment, yielding an artificial offset of 1/4 spectral width ($sw_1/4$) that was in addition to true offsets, $\nu_{off} \propto t_{off}$. Experiments with CLSW-16 used $t_{cyc} = 204$ μs, whereas LW-24 and CMG-48 had (306 μs, 100 points) and (612 μs, 100 points), respectively. All three combinations of sequence and t_{cyc} gave pulse spacings of $(\tau - t_p/2) = 6.5$ μs and RF duty cycle of ~0.314. For CLSW-16 we collected 150 complex t_1 points at $n_{incr} = 4$, whereas 100 points were collected when using LW-24 or CMG-48 at $n_{incr} = 4$ or 2, respectively. These choices maintained sequence-independent values of $t_{1,max} = 122.4$ ms (important for sequence-independent power compensation), but yielded distinct spectral widths, $sw_1 = 1.225$ kHz for CLSW-16 and 0.817 kHz for LW-24 and CMG-48. The indirect t_1 dimension was built from transients in t_2, each collected in a single scan with the first transient preceded by 20 dummy scans to ensure system equilibration. Thus, a single spectrum vs. t_1 required about (20 + 150) points for CLSW-16 or (20 + 100) or LW-24 and CMG-48, for total experiment durations of 5.0 or 3.5 min, respectively. Finally, we note two remaining details. First, to achieve full decay in t_1, collection instead to $t_{1,max} \sim 170$ ms was necessary. We verified equivalent spectral performance in such cases, but avoided the additional RF load and occasional arcing by holding to the shorter $t_{1,max}$. Also, our use of $t_p = 4.0$ μs with noted values of t_{cyc} avoided rounding errors in the timings of windows and pulses, providing all events modulo 50 ns or, when t_{off} was used, modulo ≥20 ns depending on choice of t_{off}.

2.4. Pulse programming and data analysis

Pulse sequences were programmed in house for execution in the Bruker Topspin 2.1.4 or 3.0 environments. The NMRPipe [26]

Table 3
Toggling-frame representation of CMG-48, starred values as in Tables 1 and 2.

Window	Basis ops			Quad-echo group		Window duration	Window	Basis ops			Quad-echo group		Window duration
	I_x	I_y	I_z					I_x	I_y	I_z			
0	I_x	I_y	I_z	A		τ	25[a]	I_x	I_y	I_z	A		τ
1	I_x	I_z^*	$-I_y$	B		τ	26	I_x	$-I_z^*$	I_y	−B		τ
2	I_y	I_z^*	I_x	C	C	2τ	27	$-I_y$	$-I_z^*$	I_x	C	C	2τ
3	I_y	$-I_x$	I_z		A	τ	28	$-I_y$	$-I_x$	$-I_z$		−A	τ
4	$-I_z^*$	$-I_x$	I_y	−B	−B	2τ	29	$-I_z^*$	$-I_x$	I_y	−B	−B	2τ
5	$-I_z^*$	I_y	I_x	C		τ	30	$-I_z^*$	$-I_y$	$-I_x$	−C		τ
6	$-I_x$	I_y	$-I_z$	−A	−A	2τ	31	I_x	$-I_y$	$-I_z$	−A	−A	2τ
7	$-I_x$	$-I_z^*$	$-I_y$		B	τ	32	I_x	$-I_z^*$	I_y		−B	τ
8	I_y	$-I_z^*$	$-I_x$	−C	−C	2τ	33	I_y	$-I_z^*$	$-I_x$	−C	−C	2τ
9	I_y	$-I_x$	I_z	A		τ	34	I_y	I_x	$-I_z$	−A		τ
10	I_z^*	$-I_x$	$-I_y$	B	B	2τ	35	$-I_z^*$	I_x	$-I_y$	B	B	2τ
11	I_z^*	$-I_y$	I_x		C	τ	36	$-I_z^*$	$-I_y$	$-I_x$		−C	τ
12	$-I_x$	$-I_y$	I_z	A	A	2τ	37	$-I_x$	$-I_y$	I_z	A	A	2τ
13	I_z^*	$-I_y$	I_x	C		τ	38	$-I_z^*$	$-I_y$	$-I_x$	−C		τ
14	I_z^*	$-I_x$	$-I_y$	B	B	2τ	39	$-I_z^*$	I_x	$-I_y$	B	B	2τ
15	I_y	$-I_x$	I_z		A	τ	40	I_y	I_x	$-I_z$		−A	τ
16	I_y	$-I_z^*$	$-I_x$	−C	−C	2τ	41	I_y	$-I_z^*$	$-I_x$	−C	−C	2τ
17	$-I_x$	$-I_z^*$	$-I_y$	B		τ	42	I_x	$-I_z^*$	I_y	−B		τ
18	$-I_x$	I_y	$-I_z$	−A	−A	2τ	43	I_x	$-I_y$	$-I_z$	−A	−A	2τ
19	$-I_z^*$	I_y	I_x		C	τ	44	$-I_z^*$	$-I_y$	$-I_x$		−C	τ
20	$-I_z^*$	$-I_x$	I_y	−B	−B	2τ	45	$-I_z^*$	$-I_x$	I_y	−B	−B	2τ
21	I_y	$-I_x$	I_z	A		τ	46	$-I_y$	$-I_x$	$-I_z$	−A		τ
22	I_y	I_z^*	I_x	C	C	2τ	47	$-I_y$	$-I_z^*$	I_x	C	C	2τ
23	I_x	I_z^*	$-I_y$		B	τ	48	I_x	$-I_z^*$	I_y		−B	τ
24	I_x	I_y	I_z		A	τ	49	I_x	I_y	I_z		A	τ

[a] For CMG-48, we list (n_p + 2) windows, as opposed to (n_p + 1) for CLSW-16 and LW-24 in Tables 1 and 2. This occurs because we split the central window in two (24–25). As Cory noted [9], sampling may also occur at this midpoint.

software package was used to convert Bruker-format data to text files containing raw sets of complex t_2 transients vs. time increments of a quadrature signal in t_1. Such raw data was processed and analyzed using home-written *Mathematica* code (Wolfram Research, Inc, Champaign, IL). There, transients in t_2 were multiplied by a decay-matched window function to optimize signal-to-noise, then integrated to yield 1D time-domain spectra in t_1. These were multiplied by a 3 Hz exponential window to ensure complete signal decay, then baseline corrected and Fourier transformed. Resulting lineshapes were fit to Lorentzians. Reported uncertainties of fitted parameters are the asymptotic standard error provided by *Mathematica*'s nonlinear regression routine, which is based on the Levenberg–Marquardt algorithm. Finally, for signals expected at frequencies beyond the spectral width, the fitted frequency was de-aliased by addition of the integer multiple of sw_1 bringing it nearest to the calculated values of the induced offset from zero frequency. For each sequence, this was necessary for spectra with $t_{off} \geq 125$ ns.

2.5. Numerical simulations

Calculations were performed using the SpinEvolution [27] software package (32-bit version 3.4.2) on a PC with Intel® Core™ 2 Duo Processor E8400 (3.0 GHz, 6 M, 1333 MHz FSB) and 4 GB RAM (DDR2 Non-ECC SDRAM, 800 MHz). The operating system was 32-bit Red Hat Enterprise Linux Server (release 5.5). Simulations were straightforward implementations of SpinEvolution syntax for pulse sequences [27]. Input files for the variety of MPLN sequences tested were generated from home-written *Mathematica* code. Sequences thus defined included CLSW-16, LW-24 and CMG-48 (with or without phase stepping) as functions of pulse power and/or the duration of pulse modifications for 2nd averaging. The phase-stepped versions were defined as single sequences of $4 \times n_p$ pulses, ($n_p = 16$, 24 or 48) with each n_p-pulse portion stepped 90° (or other increment) relative to its prior instance. All simulations accounted for finite pulses using $t_p = 4.0$ μs and spacings ($\tau - t_p/2$) = 6.5 μs, matching our experimentally unvarying RF duty cycle and sequence-specific t_{cyc} values. Use of $t_{1,max}$ = 122.4 ms also matched experiments.

The spin system was defined with ^{75}As as the signal nucleus at the origin of a lattice of five nearest-neighbor gallium and arsenic nuclei, as detailed in the next subsection. The initial condition of simulations was defined as $\rho = I_z^1$ and the detection operator was I_+^1, where superscripts 1 refer to the signal nucleus. Sample orientation was fixed, as for our single-crystal experiments. Resulting time-domain simulations were processed and then fit to Lorentzian shapes in the frequency domain using *Mathematica* in a manner identical to our protocols for experimental data. Because a relaxation model was not implemented in the simulations, results were multiplied by a 5 Hz exponential to ensure full decay. TPPI of the preparation pulse was not included in simulations, thus some signals appeared near zero frequency and so baseline correction was avoided.

2.6. Definition of the spin system

A critical aspect of simulations was judicious definition of the spin system. As always, the key limitation was choosing a tractable set of spins. Using SpinEvolution installed as noted, simulations were possible for up to six coupled spins 3/2. We explored corresponding selections from the GaAs lattice that would reasonably reproduce the 2.2 kHz fwhm Gaussian linewidth that we observe for ^{75}As in a static crystal. Fig. 2a displays adjacent unit cells of the lattice with arsenic signal nucleus at the origin. At six spins, a natural choice was to include two equidistant heteronuclear nearest neighbors (nn's), as well as three equidistant homonuclear

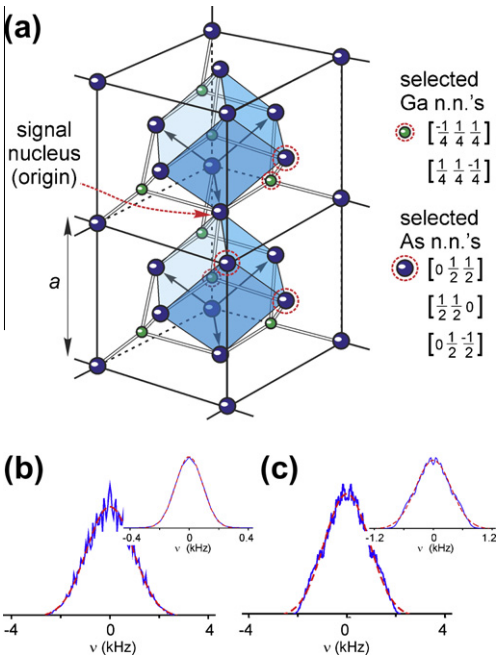

Fig. 2. GaAs structure and simulation quality. (a) Zincblende lattice, highlighting nuclei selected for accurate representation of the spin system in numerical simulations. Coordinates are specified in units of the lattice constant $a = 5.65$ Å. (b) Simulated ^{75}As NMR signal from simple $\pi/2$-detect sequence applied to system of selected spins in (a), but scaling to 0.45a. The inset shows the 10-fold narrower result using unscaled a. For each, solid blue lines connect points in the simulation, and the red, dashed curves are Gaussian fits. (c) Simulations for ^{69}Ga using a similar model, but swapping gallium and arsenic identities in the lattice, as described in the text. (For interpretation of the references to colour in this figure legend, the reader is referred to the web version of this article.)

nn's: one in-plane with the signal nucleus, one above and one below. The chosen spins were all within the same hemisphere. Simulations with this configuration and a $\pi/2$-detect sequence revealed a time-domain whose Fourier transform was a clean Gaussian. This result was obtained regardless of the heteronuclear identities as ^{69}Ga-only, ^{71}Ga-only or one of each. We proceeded with the latter as the closest representation of the 60.4/39.6 natural ratio of Ga isotopes. All $n < 6$ spin configurations tested were less satisfactory. For example, neglecting heteroatoms yielded an abrupt distortion (peaking) at the line center, whereas omitting homonuclei and instead including all four Ga nn's yields nulled heteronuclear dipolar interactions for the geometry relevant here ($\mathbf{B}_0 \parallel [0\ 0\ 1]$). That, of course, gives unrealistic, negligible linewidth.

While the chosen 6-spin representation was realistic in terms of spectral quality, a remaining imperfection is that the Gaussian line was only 200 Hz fwhm [Fig. 2b, inset] when using true atomic coordinates of GaAs. By instead scaling interatom distances such that the effective GaAs lattice constant ($a = 5.65$ Å) was reduced to 0.45a, we artificially increased dipole–dipole interactions. This produced the 2.2 kHz fwhm, approximately Gaussian shape shown in Fig. 2b. While in general agreement with experiment, this did yield a spiky character across the center of the peak. We accepted this imperfection as preferable to the overly narrow lines obtained with the natural lattice constant. For completeness and future use, we also provide an analogous model for simulation of ^{69}Ga spectra. In this case, we settled on a system of six spins with ^{69}Ga at the origin, two n.n. ^{75}As atoms and three n.n. gallium nuclei, one each above, below and in-plane with the signal nucleus. Simulations of the $\pi/2$ detect sequence in which the galliums were ^{71}Ga only or mixtures of ^{69}Ga and ^{71}Ga yielded severe oscillations across the peak, whereas using only ^{69}Ga (i.e., homonuclear) n.n.'s

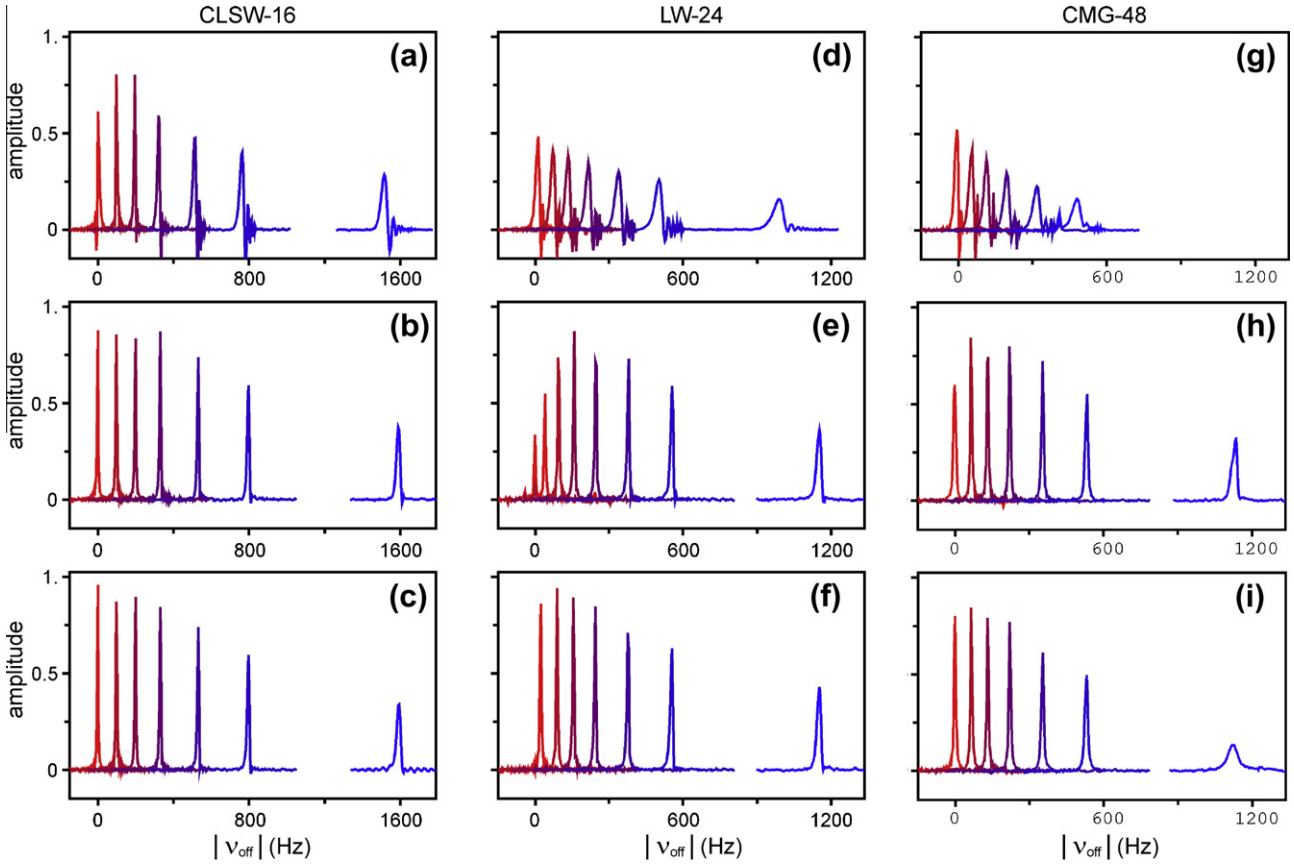

Fig. 3. Experimental line-narrowing performance. (a–c) CLSW-16, (d–f) LW-24, and (g–i) CMG-48. Individual plots are spectral series vs. $t_{off} = 0$ to ~300 ns (red-to-blue color progression). Performance of noted sequences are organized in rows as: [top (a, d, g)] without power compensation, and with power compensation, but without [middle (b, e, h)] or with [bottom (c, f, i)] phase stepping in $4 \times 90°$ steps. All spectra reflect common normalization, including account for the $\sqrt{n}$ dependence on number of points collected over given $t_{1,max}$. (For interpretation of the references to colour in this figure legend, the reader is referred to the web version of this article.)

provided a reasonably Gaussian shape. Fig. 2c presents that result at natural and scaled (0.73*a*) values of the lattice constant, yielding 0.83 and 2.17 kHz fwhm, respectively, compared to 2.14 kHz for ^{69}Ga in our experiments.

3. Results and discussion

3.1. Temporally homogeneous averaging

The power-compensation period [Fig. 1a] preceding the recycle delay (d_1) ensures that the total RF pulse energy and power demand on the RF amplifier are t_1 independent. Our implementation was inspired by similar 'temperature-compensation' pulse trains in solution-state Carr–Purcell–Meiboom–Gill relaxation experiments. For MPLN, when omitting the compensation period, the number of pulses increases linearly with t_1 and we observed severe spectral distortions. Instead of expected homogenous evolution from $\overline{\mathcal{H}}_{off}^{(0)}$, Fig. 3a, d, and g displays the distorted results from uncompensated CLSW-16, LW-24 and CMG-48, each as a function of $t_{off} = 0$ to ~300 ns. One-sided 'ringing' of the frequency domain peaks is prominent from each sequence and across the full range of t_{off} values. These artifacts are consistent with a 'chirped' evolution frequency, in which ν_{off} scales exponentially with t_1. For example, complex time-domains from each sequence were well fit by

$$S(t_1) = S_0 \exp[i(2\pi)(\nu_{off} e^{t_1/\tau_{chirp}})t_1] \quad (3)$$

where τ_{chirp} is the time constant for frequency variation in t_1. [See Fig. 4 for fitted examples from CLSW-16.] Eq. (3) is consistent with

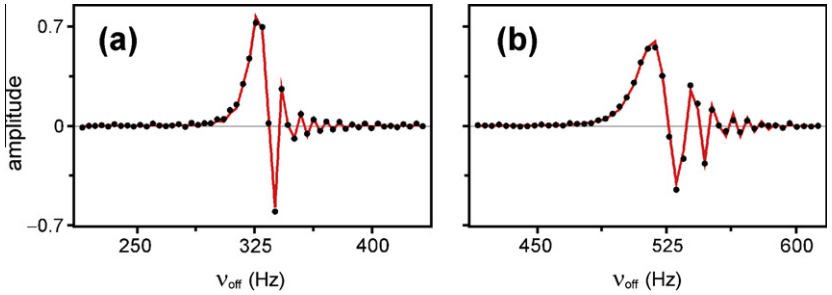

Fig. 4. Chirped frequency domain spectra from CLSW-16 without power compensation. Data (points) and fitted result (line) are shown for spectra (a) at $t_{off} = 60$ ns, yielding $\tau_{chirp} = (2.66 \pm 0.02)$ s, and (b) at $t_{off} = 100$ ns, yielding $\tau_{chirp} = (2.08 \pm 0.02)$ s. Similar quality fits were obtained for chirped data from LW-24 and CMG-48.

temporal variation of $\overline{\mathcal{H}}_{off}^{(0)}$ [Eqs. (1) and (2)] via exponential modification of the Rabi frequency (e.g., due to altered circuit response, amplifier droop, etc.).

However, that explanation is likely incomplete. First, it cannot explain the fact that fitted τ_{chirp} values vary significantly with t_{off} and sequence type: $\tau_{chirp} \sim 0.3$–11 s for CLSW-16, 0.2–1.3 s for LW-24, and 0.3–2.3 s for CMG-48, each over the noted t_{off} range. [See Fig. 4 examples.] This variation is in spite of the identical RF duty cycle used for all sequence types and t_{off} values. Additionally, chirping was apparent in t_{off}, $\overline{\mathcal{H}}_{off}^{(0)} = 0$ data sets where there was no true evolution frequency, only artificial modulation by TPPI. Finally, for all sequences, the chirped character was mitigated (perhaps 2nd averaged) in the range $t_{off} = 20$–40 ns relative to data from $t_{off} = 0$, with the distortion then growing in severity for larger t_{off}. These facts indicate that the chirping is due not only to temporal inhomogeneity of $\overline{\mathcal{H}}_{off}^{(0)}$, but also to unsuspected higher-order error terms introduced by experimental imperfections. This is especially obvious from observation of chirping when $\overline{\mathcal{H}}_{off}^{(0)} = 0$, but also from its reduction at small $\overline{\mathcal{H}}_{off}^{(0)}$, followed by return as $\overline{\mathcal{H}}_{off}^{(0)}$ grows further. Presumably, imperfections of the 2nd averaging source quickly overwhelm its benefits. For either theoretical descriptor of the distortions (t_1-dependent $\overline{\mathcal{H}}_{off}^{(0)}$ and/or the introduction of error terms), temporal dependence of B_1 is certainly a plausible mechanism.

Finally, power compensation was very effective in removing the noted artifacts. This is obvious from the results of the bottom two rows in Fig. 3. All plots in these rows were collected with power compensation, but either without [Fig. 3 (b,e,h), middle] or with phase-stepping [Fig. 3 (c, f, i), bottom]. The utility of phase stepping is the topic of the next section. Here, we emphasize that chirping is not significant in any of the power-compensated spectra from CLSW-16, LW-24 or CMG-48, regardless of either $\overline{\mathcal{H}}_{off}^{(0)}$ or implementation of phase-stepping. This is clear for data from t_{off} to ~300 ns in the bottom two rows of Fig. 3 as well as for up to $t_{off} = 1600$ ns (data not shown). The simple compensation approach should also be useful when implementing switched interactions ranging from RF or static field gradients to perturbations for POWER NMR. For example, RF electric fields proposed for measurement of NMR Stark effects in the POWER context are subject to identical factors (circuit response and amplification) of temporal variation as relevant here with RF B_1.

3.2. Combined approaches to 2nd averaging

The value of phase-stepped time-suspension sequences is emphasized by comparing results between the middle (unstepped) and bottom (stepped) rows of Fig. 3. Particular gains with phase stepping are apparent for the LW-24 [Fig. 3e and f] and CMG-48 [Fig. 3h and i] sequences. Unstepped results with either sequence do reveal good (Lorentzian) lineshapes when $\overline{\mathcal{H}}_{off}^{(0)} > 0$. However, the stepping (a) provides higher amplitude and narrower results at $t_{off} \leqslant 20$ ns, and (b) maintains performance equivalent to unstepped versions for larger t_{off} values. For CLSW-16, phase-stepping provided little-to-no benefit here [Fig. 3b and c]. However, this does not deem the stepping unproductive. Its application in less favorable circumstances (e.g., a sample with broader natural linewidth, incorporation of switched interactions, added experimental errors, etc.) may indeed be beneficial and was without harm here.

The strongest case for phase stepping is made in Fig. 5, which highlights 2nd-averaging effects with CLSW-16 in part (a), LW-24 in (b) and CMG-48 in (c). Though little effect is apparent for CLSW-16 dramatic impact on LW-24 occurred with either phase stepping or $\overline{\mathcal{H}}_{off}^{(0)}$ at $t_{off} = 60$ ns. Without 2nd averaging, the LW-24 line was split into three features about the expected position [Fig. 5b]. This cannot be explained by zeroth-order of AHT, and is therefore due to higher-order error terms. When instead using the phase stepped LW-24 at $t_{off} = 0$, the unwanted structure

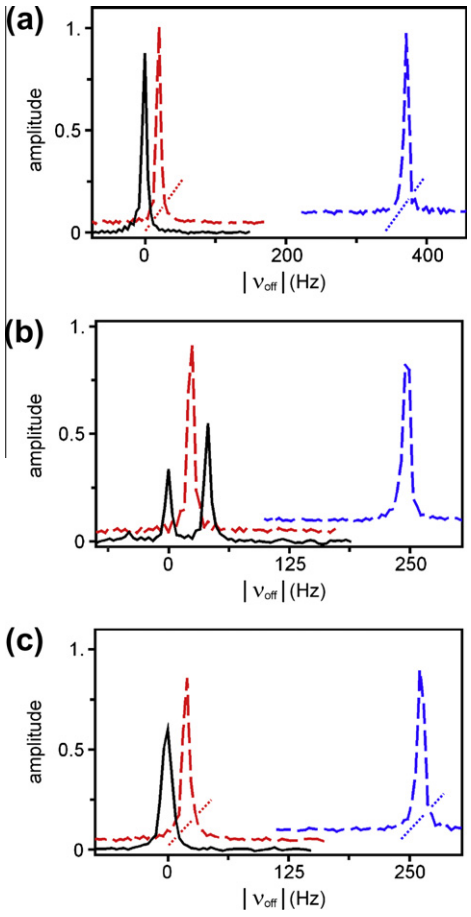

Fig. 5. Experimental enhancements of time-suspension line narrowing. From (a) CLSW-16, (b) LW-24, and (c) CMG-48. Each plot shows three spectra, all collected with power compensation: the two nearest zero frequency with $t_{off} = 0$ and either phase stepped in $4 \times 90°$ steps (red, dashed) or not (black, solid). The shifted spectrum in each plot (blue, dashed) shows unstepped data, but with $t_{off} = 60$ ns for offsets of 331, 247 and 222 Hz for the 16-, 24- and 48-pulse sequences, respectively. [All plots include artificial vertical offsets in dashed spectra for ease of viewing. For (a and c) only, a 20 Hz horizontal offset was also added, with true positions indicated by diagonal guide lines.] (For interpretation of the references to colour in this figure legend, the reader is referred to the web version of this article.)

disappeared, revealing the expected single line at >10^3-fold resolution enhancement over the natural linewidth (i.e., a fitted $\Delta\nu_{fwhm} = 1.5$ Hz). Similar performance ($\Delta\nu_{fwhm} = 2.1$–3.8 Hz) was obtained from this sequence when unstepped, but incorporating t_{off}, $\nu_{off} = 20$–60 ns, 110–250 Hz. Finally, LW-24 with combined phase stepping and $\overline{\mathcal{H}}_{off}^{(0)}$ yielded $\Delta\nu_{fwhm} = 3.3$–3.5 Hz over the same t_{off}, ν_{off} range. This indicates that (at least for the 'bare' sequence) concurrent application of these two 2nd-averaging approaches does not exceed individual benefits. However, nor does the data suggest any reason to avoid their combination.

Relative to the first two sequences, results with CMG-48 indicate an intermediate utility of 2nd averaging. The unstepped CMG-48 at $\overline{\mathcal{H}}_{off}^{(0)} = 0$ provided a poorer lineshape than any 2nd-averaged version. A fit to a single Lorentzian had $\Delta\nu_{fwhm} = 7.6$ Hz, and the spectrum hints at an unresolved splitting that was apparent when fitting the un-apodized time domain (~3.8 Hz splitting of two features each with $\Delta\nu_{fwhm} \sim 3.1$ Hz). Clearly the non-2nd-averaged CMG-48 produced contributions to the effective Hamiltonian beyond zeroth-order AHT. But as with LW-24, either phase stepping or $\overline{\mathcal{H}}_{off}^{(0)} > 0$ was sufficient to remove the artifact, and their combination maintained this efficacy. Without stepping, we obtained $\Delta\nu_{fwhm} = 2.7$–3.8 Hz for t_{off}, $\nu_{off} = 20$–60 ns, 65–220 Hz, and

with it $\Delta\nu_{fwhm}$ = 3.7–5.3 Hz for the same t_{off}, ν_{off} range. We do not feel it is of much value to comment on these slight differences (i.e., ~1–1.5 Hz broader features with stepping). Rather, we reiterate the apparent compatibility of techniques.

Full quantitative view (to $t_{off} \sim 300$ ns) of sequence performance under the variety of tested conditions is presented in Fig. 6. There, each plot tracks a parameter from Lorentzian fits over the spectral series vs. t_{off} from Fig. 2. Consistent with the prior discussion, the absence of power compensation has severe negative impact on amplitude (a_0) and linewidth ($\Delta\nu_{fwhm}$). This impact appeared less critical for CLSW-16 than with the other sequences, but in all cases this parameter-level viewpoint glosses over the added problem of chirping. Among all non-power-compensated sequences, the chirping only vanished (or nearly so) for CLSW-16 at t_{off} = 20 ns. Spectra from any sequence with power compensation all suggest performance optima (highest a_0, lowest $\Delta\nu_{fwhm}$) in the vicinity t_{off} = 20–60 ns. Beyond this range, performance consistently deteriorated. Although, we note that even at $t_{off} \sim 300$ ns, linewidths of ~12–20 Hz from the three sequences still reflect $\sim 10^2$-fold resolution enhancements over natural linewidth. Thus, the possibility of added 2nd-averaging benefits from the increased diagonal content of this 'large-t_{off}' regime should not be discounted in later applications.

Lastly, we consider the frequency offsets introduced by t_{off}, $\overline{\mathcal{H}}_{off}^{(0)} > 0$. Plots in Fig. 6c, f, and i show linear response ($\nu_{off} \propto t_{off}$) for CLSW-16, LW-24 and CMG-48. For all sequences, slopes from the two power-compensated sets (stepped or unstepped) were 6–10% higher than in the non-power-compensated case. The latter gave slopes indistinguishable from those predicted based on calibration of t_{90} [i.e., Eq. (2) with $\nu_1 = (4t_{90})^{-1}$]. It is not surprising that the slopes changed with the additional load of power-compensating pulse trains, which might affect circuit and amplifier performance, and which we used to 'smooth out' such effects across t_1. However, we did not expect the slopes to *increase* with that load. That might be explained by a fortuitous shift or narrowing of the resonance of the RF B_1 circuit, or perhaps a more exotic basis in the effect of non-t_{90} pulse times on the averaging. Nonetheless, the observation is consistent with our earlier fits to chirped signals, which similarly revealed an interaction *increasing* with the number of pulses in t_1.

An important lesson is contained within these observations. Pulse timings critically affect averaging performance [1]. Additionally, t_{90} values calibrated in standard fashion from a one-pulse experiment are not reliable when applied in the context of a MPLN sequence that totals ~20,000 such pulses at $t_{1,\max}$. Power-compensation at least keeps the total number of pulses constant, but still impacts the flip angle. It was perhaps fortuitous here that we obtained slopes (and therefore flip angles) larger than expected from naively attributed 't_{90}' values. For example, for CLSW-16 it has been shown (see pp. 65–70 of Ref. [19]) that, in order to null $\overline{\mathcal{H}}_D^{(2)}$ (the 2nd-order homonuclear dipolar contribution), one should use either the pulse angle $\beta = 90°$ or $\beta > 90°$ and a solution to

$$\delta(\beta)\left(1 - \frac{\tan\beta}{\beta}\right) = \frac{4}{3} \tag{4}$$

where $\delta(\beta) = (\beta/90°) \times (16\, t_{90}/t_{cyc})$ is the RF duty cycle. In present CLSW-16 experiments (t_{cyc} = 204 μs and t_p = 4.0 μs for fixed δ = 0.3137) the non-t_{90} optimum is expected at β = 101.5°. This corresponds to a Rabi frequency of $\sim 1.13 \times (4t_p)^{-1}$, which is similar to the ~1.08 scaling of slopes in our power-compensated CLSW-16 data vs. t_{off}. Thus, the non-power-compensated (slope consistent with $t_p = t_{90}$) and power-compensated cases ($t_p \sim 1.08 t_{90}$) both employed near-optimal pulse times. Interestingly, when reducing the RF power to obtain a slope consistent with $t_p \sim t_{90}$ in power-compensated experiments, we obtained significantly poorer line narrowing from all three sequences (data not shown).

Thus in practice, the optima suggested by Eq. (4), similar expressions for other sequences and even $t_p = t_{90}$ should all be taken as guidelines only. Calculations leading to Eq. (4) or $t_p = t_{90}$ as nulls in $\overline{\mathcal{H}}_D^{(2)}$ assumed perfectly square pulses and neglected other possible imperfections (frequency offsets, phase missets, B_1 inhomogeneity, etc.). The best approach for any sequence would seem to be empirical adjustment of the pulse power to find the largest signal amplitude at a t_1 value sufficiently sensitive to decay. For example, $t_1 = (\pi\Delta\nu_{opt})^{-1}$ would be the best choice using a guess at the true linewidth optimum ($\Delta\nu_{opt}$). Similar empirical protocols are noted in the early literature [1]. We emphasize (a) that they should be employed in a context as close as possible to the desired measurement scheme (i.e., not only with the bare sequence, but also incorporating switched interactions), and (b) that the impact of flip angle on the observed quantity (be it a frequency offset [7–9,13] or splitting [15,16]) should be evaluated as part of the measurement calibration.

3.3. Numerical simulations of idealized performance

A final goal in this paper is to evaluate the extent to which the collected MPLN spectra of Fig. 3 achieve idealized behavior of the CLSW-16, LW-24 and CMG-48 sequences. For example, are the observations of deteriorated performance for $t_{off} \geqslant 60$ ns consistent with theoretical expectations? Another key goal is to prove a simulation approach by comparing it to present data. This establishes a benchmark for later simulations of experiments that incorporate switched interactions (especially in a POWER-NMR context). AHT is either inadequate or too cumbersome to address these simple questions. Thus, we turned to numerical simulations to test the full variety of experimental cases treated above, including both techniques for 2nd averaging (phase stepping and t_{off}, $\overline{\mathcal{H}}_{off}^{(0)} > 0$). Results provide idealized expectations performance, as our simulations do not include experimental imperfections (e.g., pulse transients or B_1 inhomogeneity). Finally, we must also note that the simulations, while more exact than AHT, have their own imperfections. These are primarily due to compromises made in defining a practical representation of the spin system. As detailed in Section 2, this was adequately addressed with a choice that yielded pre-narrowed lineshapes matching the natural form and width of ^{75}As in GaAs.

MPLN simulations with ^{75}As in Figs. 7 and 8 are organized similar to experimental data in Figs. 2 and 3. Spectral progressions vs. t_{off} for the three MPLN sequences are shown in Fig. 7, either without [top row (a, c, e)] or with [bottom row (b, d, f)] phase stepping. Top/bottom plot pairs for simulations with each sequence show that phase stepping improves performance in the absence of t_{off}, $\overline{\mathcal{H}}_{off}^{(0)}$ -based 2nd averaging. This is most obvious from the amplitude dips at t_{off} = 0 in the non-stepped versions. Simulations for each sequence, with or without stepping, tend to apparent optima (tallest peaks) in the vicinity of t_{off} = 20–60 ns. Both this and the subsequent progressions to lower-amplitude, broader lines agree with our experimental results. While the plotted simulations assumed $\nu_1 = 1.08(4t_p)^{-1}$ to match experimental conditions, similar spectral profiles vs. t_{off} resulted from simulations with $\nu_1 = (4t_p)^{-1}$ (i.e., where $t_p = t_{90}$). Finally, we note that the simulated progressions of Fig. 7 extend to t_{off} = 600 ns, beyond the ~300 ns maximum included in plots of data in Fig. 3. We include the extra simulations here in order to show apparent 're-narrowing' of the lines at certain larger t_{off} values. In fact, both in experiment and simulation, we obtained spectral series extending to $t_{off} \sim 1600$ ns. Experimentally, the re-narrowing was never observed with any of the three sequences. However, other than this aspect, our simulations are in good agreement with experiment. They reproduce the utility

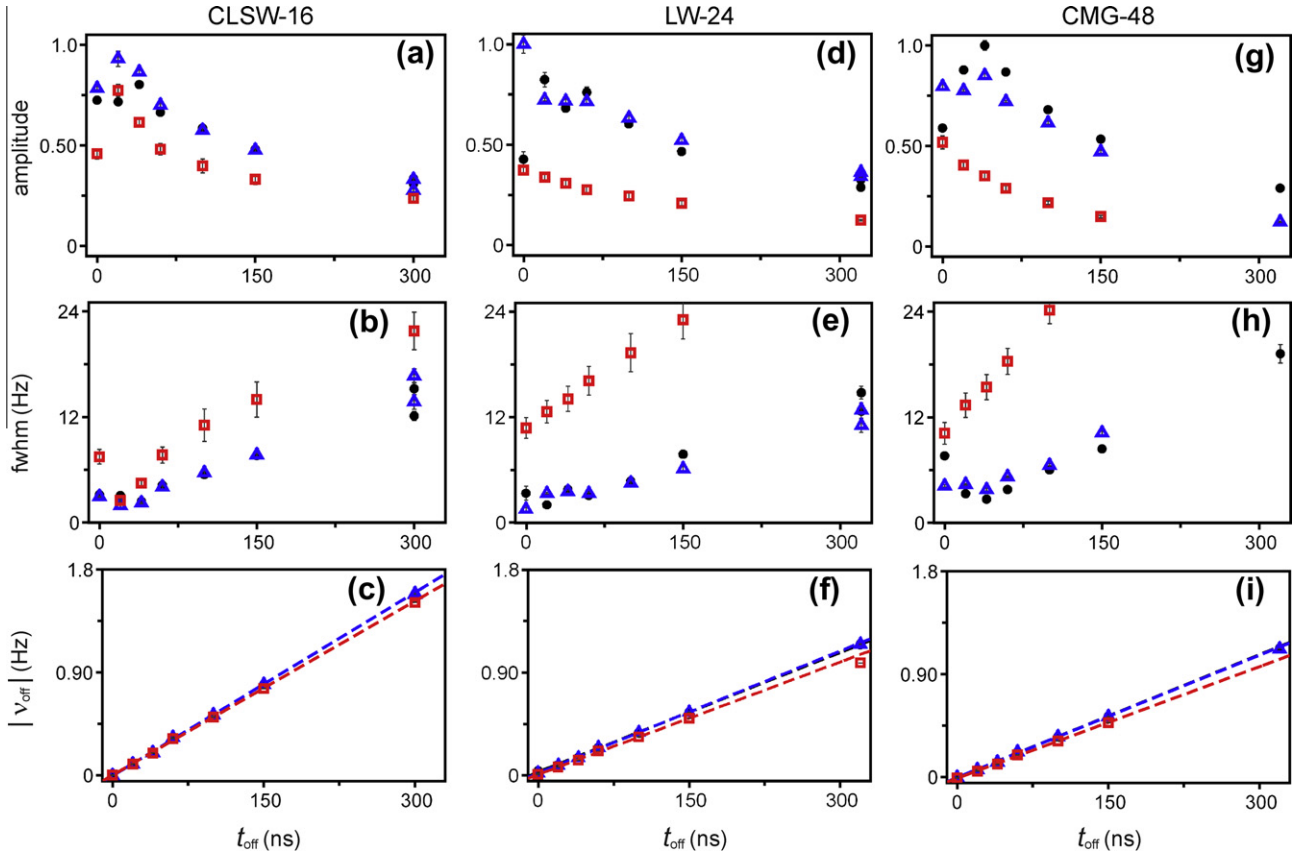

Fig. 6. Lorentzian fit parameters for spectra vs. t_{off} of Fig. 3. (a–c) CLSW-16, (d–f) LW-24, and (g–i)CMG-48. Amplitudes reflect common normalization as in Fig. 3. Each plot shows data from experiments without power compensation (red, open squares), and with power compensation, but without (black, solid circles) or with (blue, open triangles) phase stepping in 4 × 90° steps. Plots of offset frequency vs. t_{off} include linear fits (dashed lines of corresponding color). These fits excluded the highest t_{off} value in each set. Also, for each of the pulse sequences tested, fits were indistinguishable for power-compensated data with or without phase stepping. (For interpretation of the references to colour in this figure legend, the reader is referred to the web version of this article.)

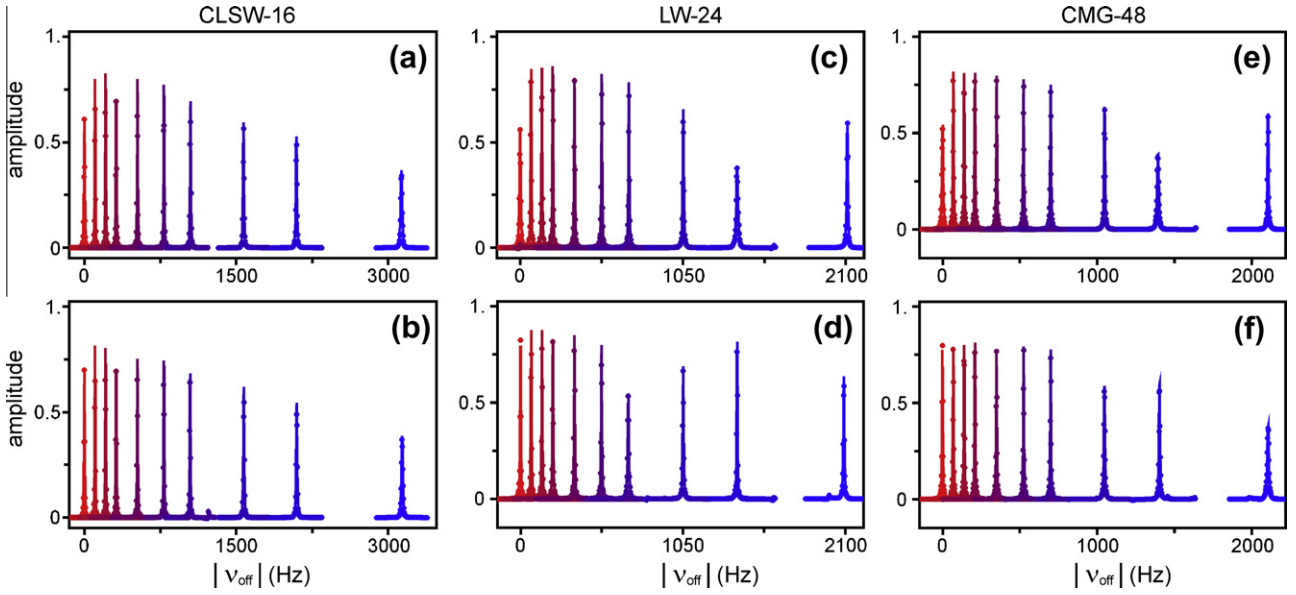

Fig. 7. Simulation of line-narrowing performance. (a and b) CLSW-16, (c and d) LW-24, and (e and f) CMG-48. Individual plots are spectral series vs. t_{off} = 0 to ~600 ns. Performance of noted sequences are organized in rows as: [top (a, c, e)] without and [bottom (b, d, f)] with phase stepping in 4 × 90° steps.

of phase stepping at t_{off} = 0, while stepped vs. unstepped trends in amplitude and linewidth (obtained from Lorenztian fits to the simulations) are indistinguishable beyond t_{off} = 20 ns (excepting occasional simulations with unexplained re-narrowing).

Fig. 8 provides close-up views of the benefits (in simulation) of both 2nd-averaging approaches, as well as the artifacts otherwise present. As for the data in Fig. 5, this shows simulation results without phase-stepping at t_{off} = 0 and 60 ns, and with it at t_{off} = 0.

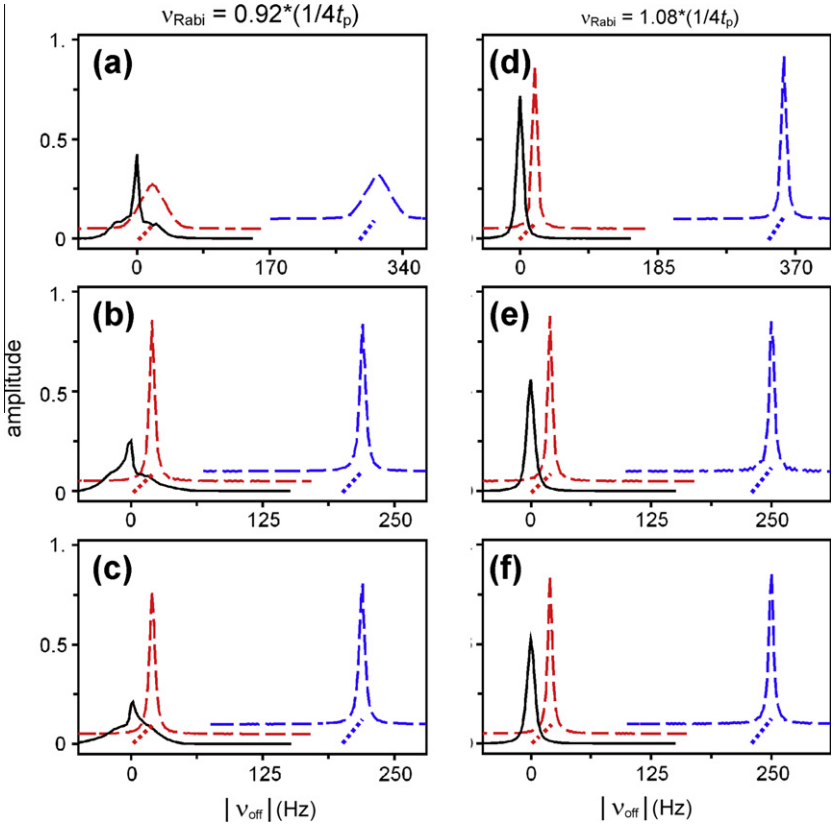

Fig. 8. Simulated time-suspension enhancements. From (a and d) CLSW-16, (b and e) LW-24, and (c and f) CMG-48. Each plot is organized as for data in Fig. 5. That is, the two simulated spectra nearest zero frequency have $t_{off} = 0$ and either phase stepped in 4 × 90° steps (red, dashed) or not (black, solid), whereas the shifted spectrum in each plot (blue, dashed) had $t_{off} = 60$ ns. Left-hand simulations (a–c) assumed ($t_p = 4$ μs) < t_{90}, whereas the right-had set (d–f) assumed ($t_p = 4$ μs) > t_{90}. Corresponding scalings of the Rabi frequency are indicated above each column. (For interpretation of the references to colour in this figure legend, the reader is referred to the web version of this article.)

A distinction is that we have simulated two cases for each time-suspension sequence: $\nu_1 = 0.92(4t_p)^{-1}$ in Fig. 8a–c and $\nu_1 = 1.08(4t_p)^{-1}$ in (d, e, f). The latter set corresponds to the experimental cases discussed above. In simulation of $\nu_1 > (4t_p)^{-1}$ cases, each of the three sequences with either phase-stepping at $t_{off} = 0$ or no stepping, but $t_{off} = 60$ ns, yielded narrower lines than in the absence of 2nd averaging. [In specific, simulations with either enhancement technique showed $\Delta\nu_{fwhm} = 2.6$–2.7 Hz for CLSW-16, <0.5 Hz for LW-24, and <0.2 Hz for CMG-48 (all after removing contributions from apodization). Unenhanced values from all sequences were 3.5–4.0 Hz.] As noted in discussion of experiments, the ∼8% increased Rabi frequency approximates the 'second' optimum of tip angle for these sequences. Thus, simulations at 8% *reduced* Rabi frequency [Fig. 8a–c] represent a greater challenge to sequence performance. For these cases, severe broadening (30 Hz width) plus zero-frequency signal distortions are apparent in all three non-2nd-averged simulations. Nonetheless, for LW-24 and CMG-48, either stepping or $t_{off} = 60$ ns was sufficient for essentially complete return to narrow lines [i.e., within 0.5–1.0 Hz of simulations at $\nu_1 = 1.08(4t_p)^{-1}$]. For CLSW-16, prospects appear to be less promising. Simulations with either 2nd-averaging approach, while restoring single Lorenztian character, did so to only a 30 Hz linewidth with this sequence. Thus, while we did not experimentally test any sequence in the $\nu_1 < (4t_p)^{-1}$ regime, the simulations suggest that LW-24 and CMG-48 may be more robust for 2nd averaging of certain experimental errors.

Finally, it is worth considering whether our phase-stepping protocol of 4 × 90° steps is the best choice. For example, if most of the averaging benefit derives from cancelation of errors on combining evolution from cycles stepped by 180°, then it would be more sensible to employ $\phi_{MPLN} = (0°, 180°)$ or perhaps to reorder the 4 × 90 steps as $\phi_{MPLN} = (0°, 180°, 90°, 270°)$, thus 'compacting' the most significant averaging benefits in time. We applied limited tests of these notions in simulations of CMG-48 with $\nu_1 = 1.08(4t_p)^{-1}$. In particular, we compared performance vs. t_{off} using phase-stepping sets of $\phi_{MPLN} = (0°, 180°)$, (0°, 90°), and (0°, 180°, 90°, 270°), along with the already discussed progression, $\phi_{MPLN} = (0°, 90°, 180°, 270°)$. For $t_{off} \geqslant 60$ ns, there were no significant distinctions among the simulations. However, predicted performance did vary for smaller t_{off}. This agrees our earlier conclusion that phase stepping is most critical when $t_{off} = 0$. There, the best enhancements were from the two arrangements of 4 × 90° steps. Both showed ∼50% higher amplitudes in the frequency domain than from the unstepped simulation. In contrast, <30% enhancement resulted using either (0°, 180°) or (0°, 90°). From this, we conclude that steps of both 90° and 180° are valuable (at least for CMG-48), and that our original 4 × 90° prescription is appropriate, with no apparent effect from step order.

In summary of simulation results, several key features of our experimental data were reproduced. These include the obvious benefits of phase-stepping at $t_{off} = 0$, the compatibility of phase-stepping and $\overline{\mathcal{H}}_{off}^{(0)}$ -based 2nd averaging across the range of tested t_{off} values, and finally the initial benefit and then decline of the latter approach. This last point is quite important. It suggests that the line narrowing we obtained in experiment approaches the best available given both present sequences and technique (i.e., stepping and pulse-timing offsets).

4. Conclusions

Present experiments and simulations provide essential tools for improving the correspondence of MPLN performance with the

zeroth-order AHT picture of spin evolution. Thorough tests of performance with three of the most well-known time-suspension sequences provide needed guidelines for use. Most notably, we found that phase-stepping alone provides as much benefit as more-traditional, $\overline{\mathcal{H}}_{off}^{(0)}$ -based 2nd averaging, and that the best results are retained when combining the two techniques. Designs for $\overline{\mathcal{H}}_{off}^{(0)} > 0$ from pulse-timing offsets were newly provided here for LW-24 and CMG-48. All three sequence designs revealed performance optima near small $t_{off} \sim 20$–60 ns (i.e., $\nu_{off} \sim 75$–250 Hz, depending on sequence, etc.). Further optimization by adjustment of pulse times or power is another well-known method, and is consistent with our observations vs. the Rabi frequency apparent during a sequence. Finally, behind all of these routes to enhancement, the constant-power technique was key for establishing temporally homogeneous averaging. With all of these approaches, a recipe emerges for extension of the present work with 'bare' sequences to those incorporating switched interactions as the dominant source of NMR evolution.

Of particular interest are measurements of switched perturbations (POWER NMR), especially double-quantum, RF Stark interactions of quadrupolar nuclei. Prior time-suspension studies focused on ^{1}H-based imaging in which I_z-based evolution was introduced by switched field gradients. While present lessons on averaging enhancements may impact that field, we expect greater significance with the more challenging POWER-NMR Stark experiments. There, the switched interaction must be converted from $I_{\pm}^2$ to an average of I_z^2 over the period of the time-suspension cycle. This is more complex and demanding than 'mere' annihilation of background spin interactions to obtain $\overline{\mathcal{H}}^{(0)} = 0$. We have developed $I_{\pm}^2 \rightarrow I_z^2$ conversion schemes with CLSW-16, LW-24 and CMG-48 (though only the first of these [15,16] is published to date). Each design is compatible with the two 2nd-averaging techniques explored here, while the constant-power approach is equally relevant for ensuring temporal homogeneity of a switched RF E field. Finally, our numerical simulations are the first step towards similar evaluation of POWER experiments. With this plus experimental options developed here, we have widened the door to a new field in which NMR may be developed as a probe of electrostatic environment.

Acknowledgments

We thank Rensselaer for financial support and Dr. Scott McCallum for instrument support. We are grateful to Dr. Werner Maas, Dr. Michael Fey and Dr. Mark Zhang of Bruker Biospin, for comments on probe design, access to related components and test equipment. We thank Dr. Mikhail Veshtort for guidance on initial setup of SpinEvolution software.

Appendix A. Supplementary material

Tabulation of phase-stepped toggling-frame operators for CLSW-16, LW-24 and CMG-48. Example derivation of $\overline{\mathcal{H}}_{off}^{(0)}$, including its invariance to phase stepping. Supplementary data associated with this article can be found, in the online version, at doi:10.1016/j.jmr.2011.01.016.

References

[1] U. Haeberlen, High Resolution NMR in Solids: Selective Averaging, Academic Press, New York, 1976.
[2] J.S. Waugh, L.M. Huber, U. Haeberlen, Approach to high-resolution NMR in solids, Phys. Rev. Lett. 20 (1968) 180–183.
[3] P. Mansfield, Symmetrized pulse sequences in high-resolution NMR in solids, J. Phys. C 4 (1971) 1944–1952.
[4] W.K. Rhim, D.D. Elleman, R.W. Vaughan, Analysis of multiple pulse NMR in solids, J. Chem. Phys. 59 (1973) 3740–3749.
[5] D.P. Burum, W.K. Rhim, Analysis of multiple pulse NMR in solids, J. Chem. Phys. 71 (1979) 944–956.
[6] D.G. Cory, A new multiple-pulse cycle for homonuclear dipolar decoupling, J. Magn. Reson. 94 (1991) 526–534.
[7] H.M. Cho, C.J. Lee, D.N. Shykind, D.P. Weitekamp, Nutation sequences for magnetic resonance imaging in solids, Phys. Rev. Lett. 55 (1985) 1923–1926.
[8] D.G. Cory, J.B. Miller, R. Turner, A.N. Garroway, Mulitiple-pulse methods of 1H-NMR imaging of solids – 2nd-averaging, Mol. Phys. 70 (1990) 331–345.
[9] D.G. Cory, J.B. Miller, A.N. Garroway, Time-suspension multiple-pulse sequences: applications to solid-state imaging, J. Magn. Reson. 90 (1990) 205–213.
[10] J.A. Marohn, D.N. Shykind, M.H. Werner, D.P. Weitekamp, Advances in multiple-pulse radio-frequency gradient imaging of solids, in: D.O. Thomson, D.E. Chimenti (Eds.), Review of Progress in Quantitative Nondestructive Evaluation, Plenum Publishing, NY, 1993, pp. 687–694.
[11] J.B. Miller, NMR imaging of materials, Prog. Nucl. Magn. Reson. Spectrosc. 33 (1998) 273–308.
[12] J.G. Kempf, J.A. Marohn, Nanoscale Fourier-transform imaging with magnetic resonance force microscopy, Phys. Rev. Lett. 90 (2003) 087601–087604.
[13] J.G. Kempf, M.A. Miller, D.P. Weitekamp, Imaging quantum confinement with optical and POWER (perturbations observed with enhanced resolution) NMR, Proc. Natl. Acad. Sci. U. S. A. 105 (2008) 20124–20129.
[14] J.G. Kempf, J.A. Marohn, P.J. Carson, J.Y. Hwang, M.A. Miller, D.A. Shykind, D.P. Weitekamp, An optical NMR spectrometer for Larmor-beat detection and high-resolution POWER NMR, Rev. Sci. Instrum. 79 (2008). 063904(1–9).
[15] J.G. Kempf, D.P. Weitekamp, Method for atomic-layer-resolved measurement of electric polarization fields by nuclear magnetic resonance, J. Vac. Sci. Technol., B 18 (2000) 2255–2262.
[16] M.R. Tarasek, J.G. Kempf, A system for NMR stark spectroscopy of quadrupolar nuclei, J. Phys. Chem. A 114 (2010) 5743–5751.
[17] M.R. Tarasek, J.G. Kempf, rf Quadrupolar NMR stark spectroscopy: steady state response and tensorial mapping, J. Phys. Chem. A 114 (2010) 10634–10645.
[18] M.H. Werner, T.J. Lenosky, D.N. Shykind, D.P. Weitekamp, ENC abstract, in: 31st Experimental NMR Conference, 1990, pp. 189.
[19] M.H. Werner, NMR Imaging of Solids with Multiple-Pulse Line Narrowing Radio Frequency Pulses, Chemistry, California Institute of Technology, Pasadena, 1993. pp. 205.
[20] A. Pines, J.S. Waugh, Quantitative aspects of coherent averaging simple treatment of resonance offset processes in multiple-pulse NMR, J. Magn. Reson. 8 (1972) 354–365.
[21] J.B. Miller, D.G. Cory, A.N. Garroway, Line-narrowing approaches to solid-state NMR imaging – pulsed gradients and 2nd averaging, Philos. Trans. R. Soc. London, A 333 (1990) 413–426.
[22] J.S. Waugh, Theory of broad-band spin decoupling, J. Magn. Reson. 50 (1982) 30–49.
[23] M.H. Levitt, R. Freeman, T. Frenkiel, Supercycles for broad-band heteronuclear decoupling, J. Magn. Reson. 50 (1982) 157–160.
[24] J.G. Kempf, Probing Quantum Confinement at the Atomic Scale with Optically Detected NMR, Chemistry, Caltech, Pasadena, CA, 2000.
[25] G. Drobny, A. Pines, S. Sinton, D.P. Weitekamp, D. Wemmer, Fourier transform multiple quantum nuclear magnetic resonance, Faraday Symp. Chem. Soc. 13 (1979) 49–55.
[26] F. Delaglio, S. Grzesiak, G. Vuister, G. Zhu, J. Pfeifer, A. Bax, NMRPipe: a multidimensional spectral processing system based on UNIX pipes, J. Biomol. NMR 6 (1995) 277–293.
[27] M. Veshtort, R.G. Griffin, SPINEVOLUTION: a powerful tool for the simulation of solid and liquid state NMR experiments, J. Magn. Reson. 178 (2006) 248–282.